Quantum mechanical modeling of the multi-stage Stern–Gerlach experiment by Frisch and Segrè using the von Neumann equation

S. Süleyman Kahraman,[1, †] Kelvin Titimbo,[1, †] Zhe He,[1] Jung-Tsung Shen,[2] and Lihong V. Wang[1, *]

[1]*Caltech Optical Imaging Laboratory, Andrew and Peggy Cherng Department of Medical Engineering,*
Department of Electrical Engineering, California Institute of Technology,
1200 E. California Blvd., MC 138-78, Pasadena, CA 91125, USA
[2]*Department of Electrical and Systems Engineering,*
Washington University in St. Louis, St. Louis, MO 63130, USA
(Dated: December 13, 2022)

The multi-stage Stern–Gerlach experiment conducted by Frisch and Segrè has been modeled analytically using quantum mechanics by Majorana and revised by Rabi by including the hyperfine interaction. However, the theoretical predictions do not match the experimental observation well. Here, we numerically solve the standard quantum mechanical model, via the von Neumann equation, that includes the hyperfine interaction for the time evolution of the spin. The outcome is compared with the experimental observation and the predictions by Majorana, Rabi, and an alternative model called co-quantum dynamics. Thus far, the coefficients of determination from the standard quantum mechanical model, which does not use free parameters, are still below zero. Non-standard variants that improve the match are explored for discussion.

Keywords: spin-flip transitions, electron spin, quantum dynamics.

I. INTRODUCTION

The Stern–Gerlach (SG) experiment [1, 2] was an essential observation in the early development of quantum mechanics and is commonly used as a segue to modern physics in most textbooks [3–5]. The SG observation was later interpreted as proof of quantization of the electron spin [6–8]. The idea of spin quantization can be more rigorously understood via multi-stage SG thought experiments [3]. The Frisch–Segrè (FS) experiment, conducted in the same lab as the first Stern–Gerlach experiment, was the first success reported [1, 9–11]. Their experiment was suggested by Einstein [7, 11, 12] and studied analytically by Majorana [13] and later by Rabi [14]. Rabi added the hyperfine interaction, which was neglected by Majorana, to modify the Majorana formula but did not explicitly solve for the evolution of the spin. However, even the improved theoretical prediction deviates from the experimental observation. Here, we numerically simulate the Frisch–Segrè experiment using a standard quantum mechanical model using the von Neumann equation without tuning the hyperfine structure coefficient and compare the outcome with the predictions by both Majorana and Rabi as well as from an alternative model called co-quantum dynamics (CQD) [15–17].

This paper is organized as follows. In Sec. II, we present the experimental configuration used by Frisch and Segrè to measure the fraction of electron spin flip. In Sec. III, we introduce the von Neumann equation and the Hamiltonian for the nuclear-electron spin system. Numerical results for the time evolution of the spins and the final electron spin flip probability are shown here. In Sec. IV, we compare the numerical results with previous solutions. Finally, Sec. V is left for conclusions. Non-standard variants of the quantum mechanical model are explored in the appendices to stimulate discussion.

II. DESCRIPTION OF THE FRISCH–SEGRÈ EXPERIMENT

The schematic used in the Frisch–Segrè experiment [9] is redrawn in Figure 1. There, magnetic regions 1 and 2 act as Stern–Gerlach apparatuses, SG1 and SG2, respectively. In SG1, stable neutral potassium atoms (^{39}K) effused from the oven are spatially separated by the magnetic field gradient according to the orientation of their electron magnetic moment $\boldsymbol{\mu}_\mathrm{e}$. The magnetically shielded space containing a current-carrying wire forms the inner rotation (IR) chamber. The shielding reduces the fringe fields from the SG magnets down to the remnant field $B_\mathrm{r} = 42\,\mu\mathrm{T}$ aligned with $+\hat{z}$. Inside the IR chamber, the current-carrying wire placed at a vertical distance z_a below the atomic beam path creates a cylindrically symmetric magnetic field. The total magnetic field in the IR chamber equals the superposition of the remnant field and the magnetic field created by the electric current I_w flowing through the wire. After SG1, the atoms enter the IR chamber; we approximate the motion to be rectilinear and constant along the y axis. Along the beam path, the magnetic field is given by

$$\mathbf{B}_\mathrm{exact} = \frac{\mu_0 I_\mathrm{w} z_\mathrm{a}}{2\pi(y^2 + z_\mathrm{a}^2)}\,\mathbf{e}_y + \left(B_\mathrm{r} - \frac{\mu_0 I_\mathrm{w} y}{2\pi(y^2 + z_\mathrm{a}^2)}\right)\mathbf{e}_z\ ,\ (1)$$

where μ_0 is the vacuum permeability; the trajectory of the atom is expressed as $y = vt$, where v is the speed of the atom and the time is set to $t = 0$ at the point on the beam path closest to the wire. The right-handed and
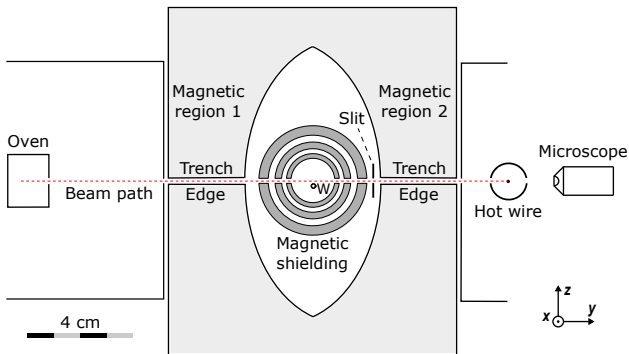
FIG. 1. Redrawn schematic of the original setup [9]. Heated atoms in the oven effuse from a slit. First, the atoms enter magnetic region 1, which acts as SG1. Then, the atoms enter the magnetic shielding (i.e., the IR chamber) containing a current-carrying wire W. Next, a slit selects one branch. Magnetic region 2 acts as SG2. The hot wire is scanned vertically to map the strength of the atomic beam along the z axis. The microscope reads the position of the hot wire.

unitary vectors $\{\mathbf{e}_x, \mathbf{e}_y, \mathbf{e}_z\}$ describe the directions of the Cartesian system.

The magnetic field inside the IR chamber has a current-dependent null point below the beam path at coordinates $(0, y_{\mathrm{NP}}, -z_{\mathrm{a}})$, with $y_{\mathrm{NP}} = \mu_0 I_{\mathrm{w}}/2\pi B_{\mathrm{r}}$. In the vicinity of the null point, the magnetic field components are approximately linear functions of the Cartesian coordinates. Hence, the magnetic field is approximated as a quadrupole magnetic field around the null point [9, 13]. Along the beam path of atoms, the approximate quadrupole field is [15, 17]

$$\mathbf{B}_{\mathrm{q}} = \frac{2\pi B_{\mathrm{r}}^2}{\mu_0 I_{\mathrm{w}}} z_{\mathrm{a}} \, \mathbf{e}_y + \frac{2\pi B_{\mathrm{r}}^2}{\mu_0 I_{\mathrm{w}}} (y - y_{\mathrm{NP}}) \, \mathbf{e}_z \; . \quad (2)$$

For the study of the time evolution of the atom inside the IR chamber both of the fields, $\mathbf{B}_{\mathrm{exact}}$ and $\mathbf{B}_{\mathrm{q}}$, are considered below.

After the IR chamber, a slit transmits one branch of electron spins polarized by SG1 and blocks the other branch. In the forthcoming theoretical model, we track only the transmitted branch with spin down at the entrance of the IR chamber and ignore the blocked branch. The atoms that reach SG2 collapse to the eigenstates for the second time and spatially separate owing to the magnetic field gradient. The final distribution of atoms is measured by scanning a hot wire along the z axis while monitored by the microscope. The probability of flip is then measured at different values of the electric current I_{w}.

III. THEORETICAL DESCRIPTION

The time evolution of the noninteracting atoms in the beam traveling through the IR chamber of the Frisch–Segrè experiment is studied using standard quantum me-

chanics. We describe the quantum system using the density operator formalism since it embodies the statistical interpretation of quantum mechanics and allows direct simulation of mixed states [18, 19]. The time evolution of the density operator $\hat{\rho}$, specifying the properties of a quantum ensemble of the system, is governed by the von Neumann equation [18, 20, 21]:

$$\frac{\partial \hat{\rho}(t)}{\partial t} = \frac{1}{i\hbar} [\hat{H}(t), \hat{\rho}(t)] \; , \quad (3)$$

where $\hat{H}(t)$ is the Hamiltonian of the system and $\hbar$ is the reduced Plank constant.

Let us consider the quantum system composed of the $4\,^2\mathrm{S}_{1/2}$ valence electron and the nucleus of the $^{39}\mathrm{K}$ atom. The interaction of the nuclear magnetic moment $\boldsymbol{\mu}_{\mathrm{n}}$ and the electron magnetic moment $\boldsymbol{\mu}_{\mathrm{e}}$ with an external magnetic field $\mathbf{B}$ is described with the Hamiltonian

$$\hat{H} = \hat{H}_{\mathrm{e}} + \hat{H}_{\mathrm{n}} + \hat{H}_{\mathrm{HFS}} \; . \quad (4)$$

First, the electron Zeeman term $\hat{H}_{\mathrm{e}}$ describes the interaction between the electron magnetic moment and the external magnetic field [22] via

$$\hat{H}_{\mathrm{e}} = -\hat{\boldsymbol{\mu}}_{\mathrm{e}} \cdot \mathbf{B} \; , \quad (5)$$

where $\hat{\boldsymbol{\mu}}_{\mathrm{e}}$ is the quantum operator for $\boldsymbol{\mu}_{\mathrm{e}}$. In $^{39}\mathrm{K}$ atoms, $\hat{\boldsymbol{\mu}}_{\mathrm{e}}$ is only due to the $4s^1$ electron with the spin angular momentum $S = 1/2$ because all other electrons are paired and the net orbital angular momentum is zero. Thus, $\hat{\boldsymbol{\mu}}_{\mathrm{e}} = \gamma_{\mathrm{e}}\hat{\mathbf{S}}$, where $\gamma_{\mathrm{e}} = -1.760\,859\,630\,23(53) \times 10^{11}\,\mathrm{rad}/(\mathrm{s\,T})$ denotes the gyromagnetic ratio of the electron; the electron spin operator $\hat{\mathbf{S}} = \frac{\hbar}{2}\hat{\boldsymbol{\sigma}}$, with the Pauli vector $\hat{\boldsymbol{\sigma}}$ consisting of the Pauli matrices $\{\sigma_x, \sigma_y, \sigma_z\}$. Substitutions yield

$$\hat{H}_{\mathrm{e}} = -\gamma_{\mathrm{e}}\frac{\hbar}{2}\,\hat{\boldsymbol{\sigma}} \cdot \mathbf{B} \; . \quad (6)$$

In the 2-dimensional Hilbert space $\mathcal{H}_{\mathrm{e}} = \mathrm{span}\,(|S, m_s\rangle)$, with $m_s = -S, \ldots, S$, the density operator of the electron spin is represented as

$$\hat{\rho}_{\mathrm{e}} = \sum_{m_s, m_s'} \rho_{m_s, m_s'} |S, m_s\rangle\langle S, m_s'| \; . \quad (7)$$

The nuclear Zeeman Hamiltonian $\hat{H}_{\mathrm{n}}$ describes the interaction of the nuclear magnetic moment with the external magnetic field:

$$\hat{H}_{\mathrm{n}} = -\hat{\boldsymbol{\mu}}_{\mathrm{n}} \cdot \mathbf{B} \; , \quad (8)$$

where $\hat{\boldsymbol{\mu}}_{\mathrm{n}} = \gamma_{\mathrm{n}}\hat{\mathbf{I}}$ denotes the quantum operator for $\boldsymbol{\mu}_{\mathrm{n}}$, γ_{n} the nuclear gyromagnetic ratio, and $\hat{\mathbf{I}}$ the nuclear spin quantum operator. For $^{39}\mathrm{K}$, the nuclear spin $I = 3/2$ and $\gamma_{\mathrm{n}} = 1.250\,061\,2(3) \times 10^7\,\mathrm{rad}/(\mathrm{s\,T})$ [23]. Therefore, we can write $\hat{\mathbf{I}} = \frac{\hbar}{2}\hat{\boldsymbol{\tau}}$, with $\hat{\boldsymbol{\tau}}$ being the generalized Pauli vector constructed with the generalized Pauli matrices for spin $3/2$, namely $\{\tau_x, \tau_y, \tau_z\}$. Substitutions produce

$$\hat{H}_{\mathrm{n}} = -\gamma_{\mathrm{n}}\frac{\hbar}{2}\,\hat{\boldsymbol{\tau}} \cdot \mathbf{B} \; . \quad (9)$$

In the 4-dimensional Hilbert space $\mathcal{H}_n = \text{span}\,(|I, m_I\rangle)$ with $m_I = -I, \ldots, I$, the density operator for the nuclear spin is

$$\hat{\rho}_n = \sum_{m_I, m_I'} \rho_{m_I, m_I'} |I, m_I\rangle\langle I, m_I'| \,. \qquad (10)$$

The interaction between the magnetic dipole moments of the nucleus and the electron gives the hyperfine structure (HFS) term $\hat{H}_{\text{HFS}}$. In terms of the electron and nuclear spin operators, the Hamiltonian is written as

$$\hat{H}_{\text{HFS}} = \frac{2\pi a_{\text{HFS}}}{\hbar} \, \hat{\mathbf{I}} \cdot \hat{\mathbf{S}} \,, \qquad (11)$$

where a_{HFS} reflects the coupling strength. For ^{39}K, a_{HFS} is set to the experimental value $a_{\text{exp}} = 230.859\,860\,1(3)$ MHz [23].

Therefore, the 8-dimensional Hilbert space for the combined nuclear–electron spin system is $\mathcal{H} = \mathcal{H}_n \otimes \mathcal{H}_e$. The tensor product combines the bases into the form $|m_I, m_s\rangle$; where for simplicity of notation we have dropped the S and I labels.

The terms of the nuclear–electron spin Hamiltonian $\hat{H} = \hat{H}_e + \hat{H}_n + \hat{H}_{\text{HFS}}$ are expressed as [24, 25]

$$
\begin{aligned}
\hat{H}_e &= -\gamma_e \frac{\hbar}{2} \, \hat{\tau}_0 \otimes (B_x \hat{\sigma}_x + B_y \hat{\sigma}_y + B_z \hat{\sigma}_z) \\
&= -\gamma_e \frac{\hbar}{2} \, \hat{\tau}_0 \otimes \begin{pmatrix} B_z & B_x - iB_y \\ B_x + iB_y & -B_z \end{pmatrix} \,, \quad (12)
\end{aligned}
$$

$$
\begin{aligned}
\hat{H}_n &= -\gamma_n \frac{\hbar}{2} \left(B_x \hat{\tau}_x + B_y \hat{\tau}_y + B_z \hat{\tau}_z \right) \otimes \hat{\sigma}_0 \\
&= -\gamma_n \frac{\hbar}{2} \begin{pmatrix} 3B_z & \sqrt{3}(B_x - iB_y) & 0 & 0 \\ \sqrt{3}(B_x + iB_y) & B_z & 2(B_x - iB_y) & 0 \\ 0 & 2(B_x + iB_y) & -B_z & \sqrt{3}(B_x - iB_y) \\ 0 & 0 & \sqrt{3}(B_x + iB_y) & -3B_z \end{pmatrix} \otimes \hat{\sigma}_0 \,, \quad (13)
\end{aligned}
$$

$$
\hat{H}_{\text{HFS}} = \frac{\pi}{2} \hbar\, a_{\text{HFS}} (\hat{\tau}_x \otimes \hat{\sigma}_x + \hat{\tau}_y \otimes \hat{\sigma}_x + \hat{\tau}_y \otimes \hat{\sigma}_z) = \frac{\pi}{2} \hbar\, a_{\text{HFS}}
\begin{pmatrix}
3 & 0 & 0 & 0 & 0 & 0 & 0 & 0 \\
0 & -3 & 2\sqrt{3} & 0 & 0 & 0 & 0 & 0 \\
0 & 2\sqrt{3} & 1 & 0 & 0 & 0 & 0 & 0 \\
0 & 0 & 0 & -1 & 4 & 0 & 0 & 0 \\
0 & 0 & 0 & 4 & -1 & 0 & 0 & 0 \\
0 & 0 & 0 & 0 & 0 & 1 & 2\sqrt{3} & 0 \\
0 & 0 & 0 & 0 & 0 & 2\sqrt{3} & -3 & 0 \\
0 & 0 & 0 & 0 & 0 & 0 & 0 & 3
\end{pmatrix} \,, \qquad (14)
$$

where $\hat{\sigma}_0$ and $\hat{\tau}_0$ are the 2-dimensional and 4-dimensional identity matrices, respectively. This Hamiltonian has been validated numerically by comparing the eigenvalues with respect to the external field with the solutions from the Breit–Rabi formula [26].

The overall density operator $\hat{\rho}$ is expressed in the basis $\{|m_I, m_s\rangle\}$ as

$$\hat{\rho} = \sum_{i,j=-I}^{I} \sum_{k,l=-S}^{S} \rho_{ik}^{jl} |i, k\rangle\langle j, l| \,. \qquad (15)$$

In the IR chamber, the external magnetic field either in the exact (1) or the quadrupole form (2) is time dependent. An exact closed-form analytical time-dependent solution for the density operator cannot be obtained. For the numerical solution of the time evolution, the von Neumann equation (3) needs to be discretized. We use the

second-order Runge–Kutta method as follows [27]:

$$\hat{\rho}(t + \frac{\Delta t}{2}) = \hat{\rho}(t) - \frac{\Delta t}{2} \frac{i}{\hbar} \left[\hat{H}(t), \hat{\rho}(t) \right] \,, \qquad (16a)$$

$$\hat{\rho}(t + \Delta t) = \hat{\rho}(t) - \Delta t \frac{i}{\hbar} \left[\hat{H}(t + \frac{\Delta t}{2}), \hat{\rho}(t + \frac{\Delta t}{2}) \right] \,, \qquad (16b)$$

where Δt is the temporal step size.

In order to solve the initial value problem, we first define the initial density operator $\hat{\rho}(t_0)$ at time t_0, corresponding to the entrance of the IR chamber. Since we track the branch with electron spin down (i.e., $|m_s = -1/2\rangle$ and $\langle \hat{S}_z \rangle = -\hbar/2$), the initial state for the electronic component is

$$\hat{\rho}_e(t_0) = \hat{\rho}_{\text{exact}}(t_0) = |-1/2\rangle\langle -1/2| = \begin{pmatrix} 0 & 0 \\ 0 & 1 \end{pmatrix} \,. \qquad (17)$$

The electron spin flips adiabatically near the wire [9, 17] to spin up, yielding $\langle \hat{S}_z \rangle = \hbar/2$. Thereafter, we numerically track the non-adiabatic flip due to the null point by considering the quadrupole approximation $\mathbf{B}_q$ shown in (2). Thus, we reset the initial state to [13, 15, 17]

$$\hat{\rho}_e(t_0) = \hat{\rho}_{\text{quad}}(t_0) = |{+}^1\!/_2\rangle\langle{+}^1\!/_2| = \begin{pmatrix} 1 & 0 \\ 0 & 0 \end{pmatrix}. \qquad (18)$$

In contrast, the initial nuclear state is assumed to be maximally mixed [14]:

$$\hat{\rho}_n(t_0) = \frac{1}{4} \begin{pmatrix} 1 & 0 & 0 & 0 \\ 0 & 1 & 0 & 0 \\ 0 & 0 & 1 & 0 \\ 0 & 0 & 0 & 1 \end{pmatrix}. \qquad (19)$$

Then, the initial density operator of the combined system is assumed to be factorized as $\hat{\rho}(t_0) = \hat{\rho}_n(t_0) \otimes \hat{\rho}_e(t_0)$.

Finally, we calculate the expectations of spin measurements, for the electron and the nucleus, in the z direction as

$$\langle \hat{S}_z \rangle = \frac{\hbar}{2} \langle \hat{\sigma}_z \rangle = \frac{\hbar}{2} \operatorname{Tr}(\hat{\rho}(t)\,\hat{\sigma}_z) , \qquad (20a)$$

$$\langle \hat{I}_z \rangle = \frac{\hbar}{2} \langle \hat{\tau}_z \rangle = \frac{\hbar}{2} \operatorname{Tr}(\hat{\rho}(t)\,\hat{\tau}_z) , \qquad (20b)$$

where Tr denotes the trace.

For the computation of the electron spin flip probability, let us introduce the projector operators $M_+ = |{+}^1\!/_2\rangle\langle{+}^1\!/_2|$ and $M_- = |{-}^1\!/_2\rangle\langle{-}^1\!/_2|$, such that they are orthogonal and span the Hilbert space for the electron spin $\mathcal{H}_e$. The operators M_+ and M_- correspond to projective measurements of electron spin $+\hbar/2$ and $-\hbar/2$, respectively. The flip probability of spin after exiting the IR chamber at time t_{end} is

$$p = \operatorname{Tr}\left(\hat{\rho}(t_{\text{end}})\,M_+\right). \qquad (21)$$

A. Excluding hyperfine interaction

We first consider the case $\hat{H} = \hat{H}_e$ by neglecting the nuclear component. The analytical asymptotic solution for this model was found using the quadrupole field approximation by Majorana [13] and applied to the Frisch–Segrè experiment [9]. Here, a numerical solution is provided for both the exact and quadrupole fields.

Figure 2a shows the evolution of $\langle \hat{S}_z \rangle$ over the flight of the atom in the IR chamber. The expectation towards the end of the IR chamber oscillates with time. As the magnetic field strength increases, the oscillation decays. Hence, we average the expectation over the final one-eighth of the flight before the exit of the IR chamber.

Figure 2b shows the flip probability of the electron spin observed in SG2 as spin up, computed using (21), for the exact and quadrupole fields at different wire currents.

(a)

(b)
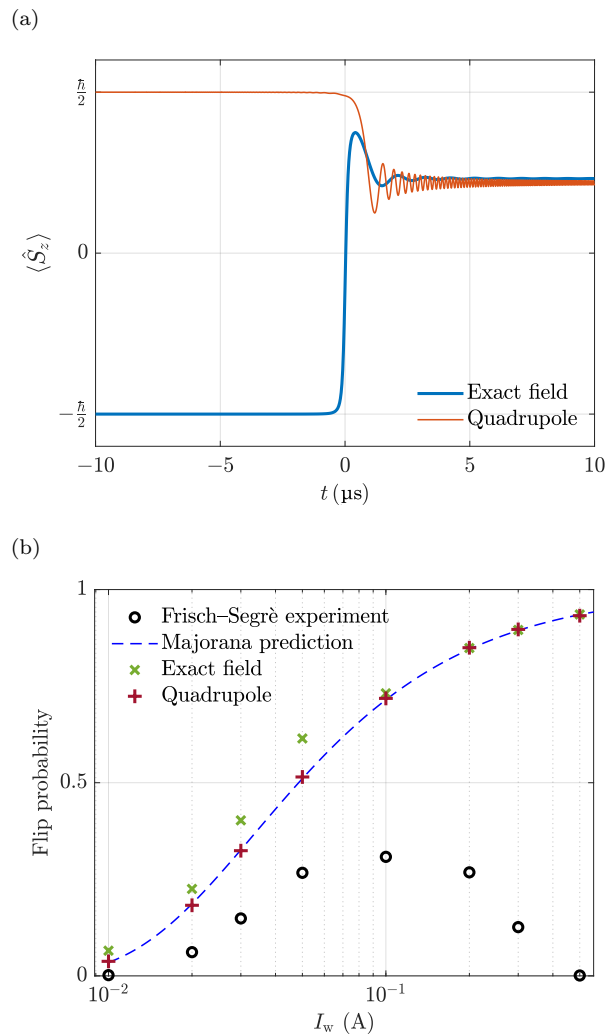
FIG. 2. (a) Time evolution of $\langle \hat{S}_z \rangle$ for the exact and quadrupole fields at wire current $I_w = 0.1\,\text{A}$. (b) Flip probability of the electron spin versus the wire current. The numerical simulations match with Majorana's prediction [13] but not with the experimental observation [9].

The numerical prediction using the quadrupole approximation agrees exactly with Majorana's analytical prediction [13] and closely with the numerical prediction using the exact field. The coefficients of determination R^2 between the numerical predictions and the experimental data are, however, -18.9 and -19.9 for the exact and quadrupole fields, respectively. Therefore, this model does not predict the experimental observation well.

B. Including hyperfine interaction

We now consider $\hat{H}$ as in (4) by including the hyperfine interaction. This model is implemented similarly as above. Figure 3a illustrates $\langle \hat{S}_z \rangle$ and $\langle \hat{I}_z \rangle$ versus the flight time of the atoms in the IR chamber for the exact field at $I_w = 0.1\,\text{A}$.

(a)

(b)
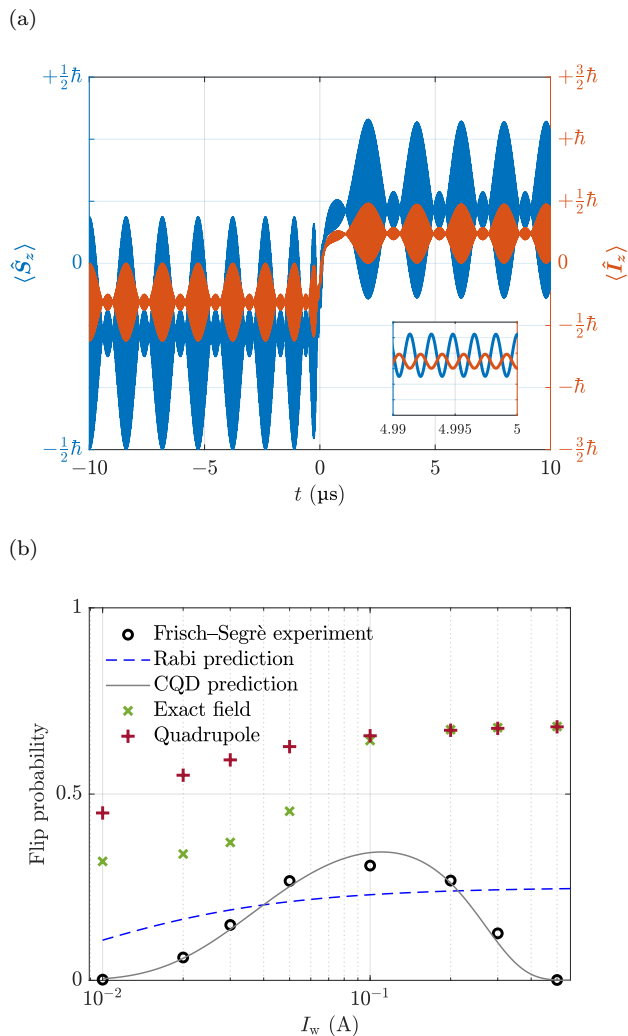
FIG. 3. (a) Evolution of $\langle \hat{S}_z \rangle$ and $\langle \hat{I}_z \rangle$ for the exact field over the flight duration within the IR chamber at $I_w = 0.1\,\text{A}$. (b) Flip probability of the electron spin for the exact and quadrupole fields when the hyperfine interaction is included. The numerical predictions do not match with the experimental observation nor with Rabi's and CQD's predictions [14, 15].

IV. DISCUSSION

In the main text, we have only considered a maximally mixed initial nuclear state as in (19), which is common in the literature [14], and have used only the experimentally measured value of a_{exp}. In the appendices, we have considered various other initial states (see Appendix A) and other values (see Appendix B). Among all the cases, the best match with the experimental observation has $R^2 = 0.51$ (see Appendix C and Table I) excluding results in Appendix D.

While one might question inaccuracies in the experiment conducted in the 1930s, a possible reason for the discrepancy is the deficiency of the models. The deficiency of Majorana's prediction is likely due to the lack of hyperfine interaction, and the deficiency of Rabi's prediction might be caused by the approximations made during his modification to the Majorana formula. Without such approximations, our numerical model that follows the standard quantum mechanical formalism should reach a higher coefficient of determination ($R^2 \sim 1$) but still does not accurately match the experimental observation. Surprisingly, recent "semi-classical" studies under CQD [15–17] have been able to match the Frisch–Segrè experimental observation well both analytically and numerically without using free parameters.

V. CONCLUSIONS

Here, we model the Frisch–Segrè experiment [9] using a standard quantum mechanical model. However, the model, which does not use free parameters, cannot predict the experimental observation well. Because the mismatch between the theory and the experiment could be due to either the model or the experiment, further investigation of both would be fruitful. In the appendices, non-standard variants of the quantum mechanical model are explored to stimulate discussion.

SUPPLEMENTAL MATERIAL

Our source codes written in Matlab are available online [28].

Figure 3b shows the flip probabilities predicted by the numerical solution in comparison to Rabi's analytical solution [14] and the experimental observation [9]. The coefficients of determination R^2 of our model for the exact and quadrupole fields in relation to the experimental observation are -11.43 and -16.27, respectively; Rabi's prediction has an $R^2 = -0.02$. Clearly, our standard quantum mechanical model or Rabi's solution, even if the HFS is considered, does not predict the experimental observation well.

Appendix A: Modified initial states

A recently developed theory called CQD [15] matches the experiment well [9] and yields an anisotropic distribution for the nuclear spin after SG1. Inspired by this work, we explore various initial states for the nuclear spin in addition to the maximally mixed state. We consider pure nuclear initial states

$$|\Psi_{\mathrm{n}}\rangle = c_1 \, |+^3/_2\rangle + c_2 \, |+^1/_2\rangle + c_3 \, |-^1/_2\rangle + c_4 \, |-^3/_2\rangle \, , \ \text{(A1)}$$

where for simplicity we constrain $c_i \in \mathbb{R}$, for $i = 1, \ldots, 4$. Then, the initial state of the compound nuclear–electron spin system is

$$\hat{\rho}_{\mathrm{pure}} = |\Psi_{\mathrm{n}}\rangle\langle\Psi_{\mathrm{n}}| \otimes \hat{\rho}_{\mathrm{e}}(t_0) \, . \quad \text{(A2)}$$

Also, we consider a family of mixed nuclear initial states with all off-diagonal elements set to zero. Thus, the initial state for the compound system reads

$$\hat{\rho}_{\mathrm{mixed}} = \begin{pmatrix} d_1 & 0 & 0 & 0 \\ 0 & d_2 & 0 & 0 \\ 0 & 0 & d_3 & 0 \\ 0 & 0 & 0 & d_4 \end{pmatrix} \otimes \hat{\rho}_{\mathrm{e}}(t_0) \, . \quad \text{(A3)}$$

Some of the tested pure states include $(c_1, c_2, c_3, c_4) \propto$ $(1, 1, 1, 1)$, $(0, 1, 2, 3)$, $(1, 0, 0, 1)$, $(1, 0, 0, \sqrt{2})$, and $(1, 0, 0, \sqrt{3})$. Meanwhile, some of the tried mixed states include $(d_1, d_2, d_3, d_4) \propto (1, 1, 1, 1)$, $(0, 1, 2, 3)$, $(1, 0, 0, 1)$, $(1, 0, 0, 2)$, and $(1, 0, 0, 3)$.

Appendix B: Modified HFS coefficients

Up to now, we have used the experimentally measured HFS coefficient value, $a_{\mathrm{exp}} = 230.859\,860\,1(3)\,\mathrm{MHz}$ [23], which does not accurately predict the experimental observation by Frisch and Segrè. Here, we modify the hyperfine coefficient to improve the match.

One way to calculate the HFS coefficient is to use the Fermi contact interaction as follows [22, 24, 29, 30]:

$$2\pi\hbar \, a_{\mathrm{HFS}} = -\hbar^2 \frac{2\mu_0}{3} \gamma_{\mathrm{e}} \gamma_{\mathrm{n}} |\psi(0)|^2 \, , \quad \text{(B1)}$$

where $\psi(\mathbf{r})$ denotes the wave function of the electron. The wave function for the $4s^1$ electron in $^{39}\mathrm{K}$ does not have an exact solution. However, various approximations are available [15, 31, 32], yielding the following HFS coefficients:

$$a_1 = -\hbar \frac{\mu_0 \gamma_{\mathrm{e}} \gamma_{\mathrm{n}}}{4\pi^2 R^3} \approx 355\,\mathrm{kHz} \, , \quad \text{(B2a)}$$

$$a_2 = -\hbar \frac{8\mu_0 \gamma_{\mathrm{e}} \gamma_{\mathrm{n}}}{3\pi^4 R^3} \approx 384\,\mathrm{kHz} \, , \quad \text{(B2b)}$$

$$a_3 = -\hbar \frac{28.4\mu_0 \gamma_{\mathrm{e}} \gamma_{\mathrm{n}}}{6\pi^2 R^3} \approx 6.72\,\mathrm{MHz} \, , \quad \text{(B2c)}$$
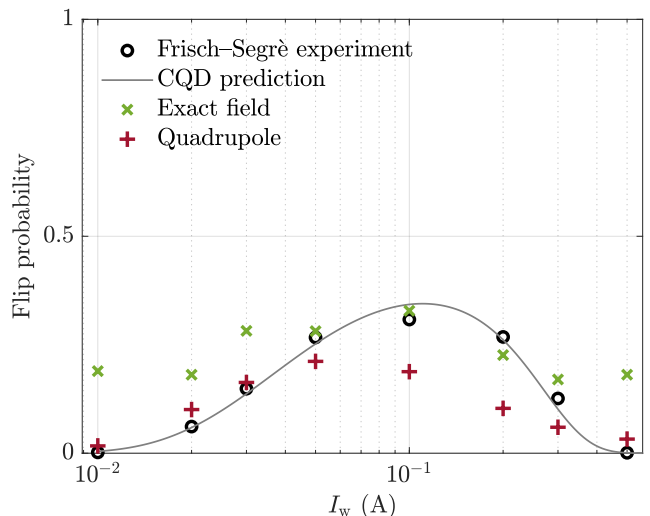
FIG. 4. Flip probability of the electron spin versus the wire current for both the exact and quadrupole fields. Only the best matches of the theoretical predictions with the experimental observation are plotted, and the corresponding parameters are included in Table I.

where $R = 275\,\mathrm{pm}$ is the van der Waals radius for $^{39}\mathrm{K}$. Another set of values for a_{HFS} are obtained on the basis of an alternative averaging method [15]:

$$a_4 = -\hbar \frac{5\mu_0 \gamma_{\mathrm{e}} \gamma_{\mathrm{n}}}{32\pi^2 R^3} \approx 222\,\mathrm{kHz} \, , \quad \text{(B3a)}$$

$$a_5 = -\hbar \frac{2\mu_0 \gamma_{\mathrm{e}} \gamma_{\mathrm{n}}}{3\pi^4 R^3} \approx 95.9\,\mathrm{kHz} \, , \quad \text{(B3b)}$$

$$a_6 = -\hbar \frac{0.138\mu_0 \gamma_{\mathrm{e}} \gamma_{\mathrm{n}}}{2\pi^2 R^3} \approx 98.0\,\mathrm{kHz} \, . \quad \text{(B3c)}$$

All of these values along with the experimental value, a_{exp}, have been tried.

Appendix C: Selected outcomes

Table I and Figure 4 show the matches with the highest R^2 among the tested cases. Among all the initial density matrices and the HFS coefficients considered, the combination of the maximally distributed pure initial nuclear state and a_2 matches the experiment the closest under the exact field. Under the quadrupole field, the closest match is from the combination of the anisotropic pure initial nuclear state and a_4.

Ideally, one should sample all feasible density matrices for a 4-state spin system and try each case with experimental and theoretical HFS coefficients along with other possible values. However, even if the Frisch–Segrè data can be matched for a specific initial state, one should still explain how such a state can be obtained through SG1. The cases considered in this paper are the simplest cases one might think of, and the results do not match well with the experimental observation.

TABLE I. Coefficients of determination (R^2) for the flip probabilities with respect to the experimental observation for various HFS coefficients.

Initial state	Magnetic field	a_{exp}	a_2	a_4
$\hat{\rho}_{\mathrm{n}}(t_0) = \frac{1}{4}\begin{pmatrix} 1&0&0&0 \\ 0&1&0&0 \\ 0&0&1&0 \\ 0&0&0&1 \end{pmatrix}$	exact	-11.43	-2.47	-2.54
	quadrupole	-16.27	-0.55	-1.41
$\lvert\Psi_{\mathrm{n}}(t_0)\rangle = \frac{1}{2}\big(\lvert+^3/_2\rangle + \lvert+^1/_2\rangle$ $+ \lvert-^1/_2\rangle + \lvert-^3/_2\rangle\big)$	exact	-11.58	**0.01**	-5.99
	quadrupole	-16.70	-0.20	0.01
$\lvert\Psi_{\mathrm{n}}(t_0)\rangle = \frac{1}{\sqrt{14}}\big(0\lvert+^3/_2\rangle + 1\lvert+^1/_2\rangle$ $+ 2\lvert-^1/_2\rangle + 3\lvert-^3/_2\rangle\big)$	exact	-16.74	-0.76	-4.38
	quadrupole	-9.78	-0.54	**0.51**

Appendix D: Non-quantum mechanical squared probabilities

Recent studies using CQD [15, 16] that match the Frisch–Segrè experiment well derived the flip probability equal to the square of the quantum mechanical counterpart. The squaring is due to an anisotropic distribution of the nuclear spin produced by the first Stern–Gerlach stage [15]. Here, we translate the anisotropic distribution to

$$\hat{\rho}_{\mathrm{n}}(t_0) = \frac{1}{3}\begin{pmatrix} 1&0&0&0 \\ 0&0&0&0 \\ 0&0&0&0 \\ 0&0&0&2 \end{pmatrix}. \tag{D1}$$

Further, we use a_4 to be consistent with CQD and include a_{exp} for comparison. The numerical outcome matches the experimental observation well, yielding coefficients of determination of $R^2 = 0.81$ for the exact field and $R^2 = 0.73$ for the quadrupole approximation, as shown in Table II and Figure 5. Although this modification is not justified under quantum mechanics, we report the result to stimulate discussion.

TABLE II. Coefficients of determination (R^2) for the artificially squared flip probabilities with respect to the experimental observation for two different HFS coefficients.

Initial state	Magnetic field	a_{exp}	a_4
$\hat{\rho}_{\mathrm{n}}(t_0) = \frac{1}{3}\begin{pmatrix} 1&0&0&0 \\ 0&0&0&0 \\ 0&0&0&0 \\ 0&0&0&2 \end{pmatrix}$	exact	-10.81	0.61
	quadrupole	-6.34	0.69
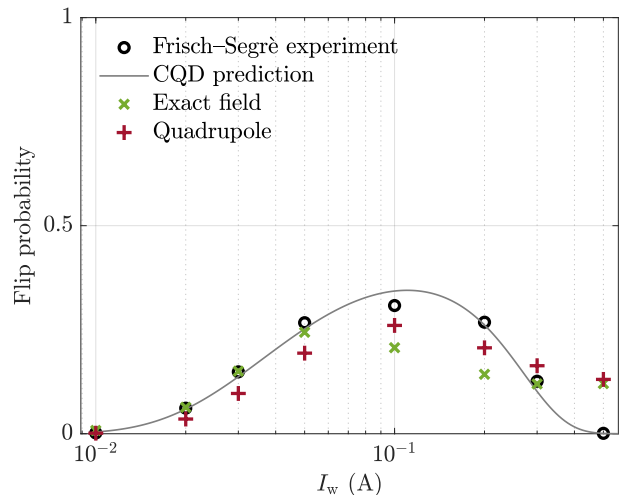
FIG. 5. Squared flip probability of the electron spin versus the wire current for both the exact and quadrupole fields. Only the theoretical predictions using a_4 are plotted, and the corresponding R^2 values are listed in Table II.

[1] W. Gerlach and O. Stern, Der experimentelle nachweis des magnetischen moments des silberatoms, Z. Phys. **8**, 110 (1922).

[2] W. Gerlach and O. Stern, Über die richtungsquantelung im magnetfeld, Ann. Phys. **379**, 673 (1924).

[3] J. J. Sakurai and J. Napolitano, *Modern Quantum Mechanics*, 2nd ed. (Addison-Wesley, 2011).

[4] R. P. Feynman, R. B. Leighton, and M. L. Sands, *The Feynman Lectures on Physics*, Vol. III: Quantum Mechanics (Basic Books, 2011).

[5] A. Messiah, *Quantum Mechanics* (Dover Publications, Inc, 2020).

[6] G. Uhlenbeck and S. Goudsmit, Ersetzung der hypothese vom unmechanischen zwang durch eine forderung bezüglich des inneren verhaltens jedes einzelnen elektrons, Naturwissenschaften **13**, 953 (1925).

[7] H. Schmidt-Böcking, L. Schmidt, H. J. Lüdde, W. Trageser, A. Templeton, and T. Sauer, The Stern–Gerlach experiment revisited, Eur. Phys. J. H **41**, 327 (2016).

[8] D. Castelvecchi, The Stern–Gerlach experiment at 100, Nat. Rev. Phys. **4**, 140 (2022).

[9] R. Frisch and E. Segrè, Über die einstellung der richtungsquantelung. II, Z. Phys. **80**, 610 (1933).

[10] T. E. Phipps and O. Stern, über die Einstellung der Richtungsquantelung, Zeitschrift für Physik **73**, 185 (1932).

[11] B. Friedrich and H. Schmidt-Böcking, eds., *Molecular Beams in Physics and Chemistry: From Otto Stern's Pioneering Exploits to Present-Day Feats* (Springer, 2021).

[12] H. Schmidt-Böcking, A. Templeton, and W. Trageser, eds., *Otto Sterns gesammelte Briefe – Band 2: Sterns wissenschaftliche Arbeiten und zur Geschichte der Nobelpreisvergabe* (Springer, 2019).

[13] E. Majorana, Atomi orientati in campo magnetico variabile, Il Nuovo Cimento **9**, 43 (1932).

[14] I. I. Rabi, On the process of space quantization, Phys. Rev. **49**, 324 (1936).

[15] L. V. Wang, Multi-stage Stern-Gerlach experiment modeled (2022), 2208.06471 [quant-ph].

[16] Z. He, K. Titimbo, D. C. Garrett, S. S. Kahraman, and L. V. Wang, Numerical modeling of the multi-stage Stern–Gerlach experiment by Frisch and Segrè using co-quantum dynamics via the Schrödinger equation, arXiv 10.48550/arxiv.2208.14588 (2022).

[17] K. Titimbo, D. C. Garrett, S. S. Kahraman, Z. He, and L. V. Wang, Numerical modeling of the multi-stage Stern–Gerlach experiment by Frisch and Segrè us-

[18] ing co-quantum dynamics via the Bloch equation, arXiv 10.48550/arxiv.2208.13444 (2022).

[19] J. von Neumann, *Mathematische Grundlagen der Quantenmechanik* (Springer, 1932).

[19] J. von Neumann, *Mathematical Foundations of Quantum Mechanics*, edited by N. A. Wheeler (Princeton University Press, 2018).

[20] R. Alicki and M. Fannes, *Quantum Dynamical Systems* (Oxford University Press, 2001).

[21] F. Benatti, *Dynamics, Information and Complexity in Quantum Systems*, Theoretical and Mathematical Physics (Springer, 2009).

[22] D. J. Griffiths and D. F. Schroeter, *Introduction to Quantum Mechanics* (Cambridge University Press, 2018).

[23] E. Arimondo, M. Inguscio, and P. Violino, Experimental determinations of the hyperfine structure in the alkali atoms, Rev. Mod. Phys. **49**, 31 (1977).

[24] M. H. Levitt, *Spin Dynamics: Basics of Nuclear Magnetic Resonance*, 2nd ed. (John Wiley & Sons, 2008).

[25] R. Schmied, *Using Mathematica for Quantum Mechanics* (Springer, 2020).

[26] G. Breit and I. I. Rabi, Measurement of nuclear spin, Phys. Rev. **38**, 2082 (1931).

[27] E. Süli and D. F. Mayers, *An Introduction to Numerical Analysis* (Cambridge University Press, 2003).

[28] S. S. Kahraman, K. Titimbo, Z. He, and L. V. Wang, Quantum mechanical modeling of the multi-stage Stern–Gerlach experiment by Frisch and Segrè using the von Neumann equation, GitHub (2022).

[29] E. Fermi, Magnetic moments of atomic nuclei, Nature **125**, 16 (1930).

[30] J. D. Jackson, *Classical Electrodynamics*, 3rd ed. (Wiley, 1999).

[31] D. R. Hartree, Results of calculations of atomic wave functions. II.— Results for K^+ and Cs^+, Proc. R. Soc. Lond. A **143**, 506 (1934).

[32] H. C. Ohanian, What is spin?, Am. J. Phys. **54**, 500 (1986).